Influence of dephasing on the Akaike-information-criterion distinguishing of quantum interference and Autler–Townes splitting in coherent systems

Jinhong Liu,[1] ⓘ Jinze Wu,[1,2] ⓘ Yueying Zhang,[2] Yanyan He,[2] and Junxiang Zhang[2,*]

[1]*State Key Laboratory of Quantum Optics and Quantum Optics Devices, Institute of Opto-Electronics, Shanxi University, Taiyuan 030006, China*
[2]*Interdisciplinary Center of Quantum Information, State Key Laboratory of Modern Optical Instrumentation, and Zhejiang Province Key Laboratory of Quantum Technology and Device of Physics Department, Zhejiang University, Hangzhou 310027, China*
*Corresponding author: junxiang_zhang@zju.edu.cn

Electromagnetically induced transparency is a quantum interference (QI) effect in a coherent system, in which the similar but distinct effect of Autler–Townes splitting (ATS) without QI also happens concurrently. The Akaike information criterion (AIC) has been proven to be an efficient and objective method to discern them by evaluating their relative AIC weights for different Rabi frequencies of the coupling field. Here, we investigate in detail the influence of the dephasing effect on the AIC weights of QI and ATS, and present the transition among destructive QI, constructive QI, and ATS without QI by controlling the dephasing rates. By comparing the effects of different dephasing rates on the QI and ATS weights, we show that the field-phase-diffusion dephasing provides more feasibility than the atom-collision dephasing in control of QI and ATS. Therefore, precise and selective dephasing engineering can be realized by manipulating the linewidths and phase correlation of the fields. This indicates that various collision-related effects (e.g., collision-dephasing-induced coherences) can be experimentally studied using more controllable field-phase-diffusion dephasing instead of buffer-gas-controlling collision dephasing.   © 2019 Optical Society of America

1. INTRODUCTION

The interaction of atomic ensemble with fields shows a variety of fascinating phenomena such as electromagnetically induced transparency (EIT) [1–3] and has potential applications in quantum information processing [4,5] and quantum engineering [6–8]. Since the optical properties of EIT media can be greatly modified and controlled by the coupling field, the EIT-related effects have been widely used for active and quantum control of light, such as slow light propagation [9,10], light storage and quantum memory [11–15], nonclassical light preparation [16–19], giant Faraday rotation [20], and tunable optical buffer [21].

Generally, EIT is a joint effect of quantum interference (QI) and Autler–Townes splitting (ATS) in an atomic system driven by a coupling field [22–25], which splits the excited state into two dressed states. QI occurs between the two excitation pathways, leading to a narrow and deep transparent window, i.e., EIT effect. When the Rabi frequency of the coupling field is

much larger than decay rates, QI can be neglected due to well-separated dressed states, and the probe absorption spectrum is just a superposition of two Lorentzian profiles with a wide transparent window, i.e., ATS effect [26,27]. Due to the wide transparency window and the reversible transfer of atomic spin and photonic coherences, ATS has been used for laser cooling [28], high-resolution spectroscopy [29,30], and especially for high-speed and broadband storage of photons [31].

Both EIT and ATS create transparency windows but the underlying mechanisms are different. The narrow and deep transparency window in EIT is due to QI, while the much wider one in ATS is just a result of the well-separated dressed states. The Rabi frequency of the coupling field is responsible for discerning these two similar but distinct effects, and the very weak (or strong) coupling field gives rise to EIT (or ATS) [24,25,32]. In most cases in which the Rabi frequency is comparable to the decay rates, the crossover between EIT and ATS occurs and remains an active topic [33–36].

Recently, an objective method based on the Akaike information criterion (AIC) [37,38] was proposed to discern EIT and

ATS [24], and it allows one to quantitatively determine the relative weights of EIT and ATS from experimental spectra, without the knowledge of any experimental parameter. Moreover, this method sets a threshold of the coupling Rabi frequency, Ω_{th}, to characterize the transition from EIT to ATS as the Rabi frequency increases. Due to its feasibility in experiments, the AIC method has been successfully employed in whispering-gallery microcavities [34], plasmonic waveguide and coupled resonator systems [35], circuit quantum electrodynamics systems [36], etc.

Apart from the Rabi frequency, which creates the atomic coherence, the dephasing is also an important and inevitable process. In general, dephasing arises from perturbations by the environment and destroys the atomic coherence, which results in EIT [1]. It has been shown that collisional dephasing can lead to the transition from EIT to electromagnetically induced absorption (EIA) [39]. Atomic collisions also result in the loss of spin angular momentum to the motional angular momentum and being destroyed, which broadens the magnetic linewidth [40–42]. Thus, it is expected that dephasing plays a key role in the study of the transition between EIT and ATS.

In this paper, we study in detail the influences of various dephasings on AIC-based distinguishing of QI and ATS, and highlight the crucial role of dephasing. We show that dephasing can lead to the transition among destructive QI (EIT), constructive QI (EIA), and ATS without QI. When one uses AIC to differentiate EIT (EIA) and ATS, not only the coupling Rabi frequency but also the dephasing rates should be considered. Furthermore, compared to the Rabi frequency, the dephasing provides more degrees of freedom to control the AIC weights of QI and ATS. By comparing different dephasing effects, we show that the field-phase-diffusion dephasing has much more feasibility than the atom-collision dephasing in control of QI and ATS. More importantly, we show that the correlation or anti-correlation between the phases of the coupling and probe fields is crucial to enhance QI or ATS. Our work highlights the crucial role of dephasing in manipulation of QI and ATS for various quantum engineering applications.

2. DEPHASING OF THE ATOM–FIELD INTERACTION SYSTEM

We consider a Λ-type three-level system with one excited and two lower states, as shown in Fig. 1(a). It is driven by a coupling field $E_c = \mathcal{E}_c e^{-i\omega_c t - i\phi_c(t)}$ and a probe field $E_p = \mathcal{E}_p e^{-i\omega_p t - i\phi_p(t)}$ with amplitude $\mathcal{E}_{c(p)}$, angular frequency $\omega_{c(p)}$, and phase $\phi_{c(p)}(t)$. This system can be found, e.g., in the D1 line of ^{133}Cs for $|e\rangle = |6P_{1/2}, F = 4\rangle$, $|m\rangle = |6S_{1/2}, F = 4\rangle$, and $|g\rangle = |6S_{1/2}, F = 3\rangle$ [43]. The
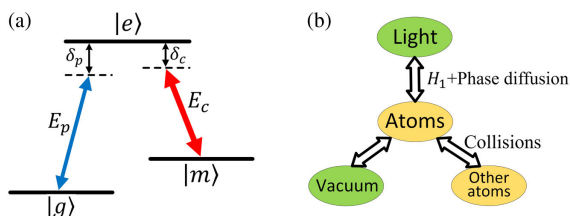

Fig. 1. (a) Atom–field system. (b) Mechanism of decoherence in atoms.

spontaneous decay rates from $|e\rangle$ to $|m\rangle$ and $|g\rangle$ are Γ_{em} and Γ_{eg}, respectively, and the total spontaneous decay rate of $|e\rangle$ is $\Gamma = \Gamma_{em} + \Gamma_{eg}$ ($= 2\pi \times 4.56$ MHz for ^{133}Cs D1 line). The detunings of the coupling and probe fields are $\delta_c = \omega_e - \omega_m - \omega_c$ and $\delta_p = \omega_e - \omega_p$, respectively, with $\omega_{e(m)}$ the frequency of $|e\rangle(|m\rangle)$ with respect to a zero reference frequency of $|g\rangle$.

In this system, the interaction of atoms with fields induces the atomic coherence, which is usually destroyed by the environment, i.e., the atoms experience decoherence. This decoherence is caused mainly by atom–atom collisions, and vacuum and field fluctuations [see Fig. 1(b)]. The Hamiltonian of the system is ($\hbar = 1$)

$$H = [\omega_e + \delta\omega_e(t)]\sigma_{ee} + [\omega_m + \delta\omega_m(t)]\sigma_{mm}$$
$$- \Omega_c e^{-i\omega_c t - i\phi_c(t)}\sigma_{em} - \Omega_p e^{-i\omega_p t - i\phi_p(t)}\sigma_{eg} + \text{H.c.,}$$
(1)

with $\sigma_{ij} = |i\rangle\langle j|(i, j = e, m, g)$. $\Omega_{c(p)} = d_{em(eg)}\mathcal{E}_{c(p)}$ is the Rabi frequency of the coupling (probe) field, and $d_{em(eg)}$ is the dipole matrix element of the transition $|e\rangle \leftrightarrow |m\rangle(|g\rangle)$.

The atomic collisions give rise to the random shifts $\delta\omega_e(t)$ and $\delta\omega_m(t)$ of $|e\rangle$ and $|m\rangle$, respectively [44–46], resulting in the decoherence of atoms. They are independent of each other and can be described by δ-correlated Gaussian stochastic processes with

$$\langle \delta\omega_{e(m)}(t) \rangle = 0,$$
(2a)

$$\langle \delta\omega_{e(m)}(t_1)\delta\omega_{e(m)}(t_2) \rangle = 2\gamma_{e(m)}^{(d)}\delta(t_1 - t_2),$$
(2b)

$$\langle \delta\omega_e(t_1)\delta\omega_m(t_2) \rangle = 0,$$
(2c)

where $\gamma_{e(m)}^{(d)}$ is the auto-correlation coefficient. In the following discussion, we will prove that the collisional dephasing rate equals $\gamma_{e(m)}^{(d)}$. This atomic-collision-induced dephasing occurs in the atomic vapor cell with buffer gas. For the case of an anti-relaxation cell, the decoherence mechanism is different [40].

Apart from the collision-induced decoherence, the fluctuations of interacting fields also induce decoherence. In general, both the amplitude $\mathcal{E}_{c(p)}$ and phase $\phi_{c(p)}$ of the field exhibit random fluctuations due to the spontaneous emission in the gain medium of a laser. However, if the laser is operating sufficiently far above threshold, the amplitude fluctuation can be ignored, and the field can be described by the phase diffusion model [47], in which $\phi_{c(p)}(t)$ undergoes diffusion: $\dot{\phi}_{c(p)}(t) = \mu_{c(p)}(t)$, with

$$\langle \mu_{c(p)}(t) \rangle = 0,$$
(3a)

$$\langle \mu_{c(p)}(t_1)\mu_{c(p)}(t_2) \rangle = 2\kappa_{c(p)}^{(d)}\delta(t_1 - t_2),$$
(3b)

$$\langle \mu_c(t_1)\mu_p(t_2) \rangle = 2\zeta_{cp}\sqrt{\kappa_c^{(d)}\kappa_p^{(d)}}\delta(t_1 - t_2),$$
(3c)

where the phase-diffusion rate $2\kappa_{c(p)}^{(d)}$ equals the linewidth of the field, and $\zeta_{cp} \in [-1, 1]$ is the Pearson correlation coefficient [48,49]. $\zeta_{cp} > 0$ ($\zeta_{cp} < 0$) denotes the correlation (anti-correlation) between the phases of the coupling and probe fields.

Generally, atomic collisions and field phase diffusions are two independent processes, and thus we have

$$\langle \delta\omega_{e(m)}(t_1)\mu_{c(p)}(t_2)\rangle = 0. \tag{4}$$

Introducing a unitary transformation $U(t) = \sigma_{ee} + e^{-i\omega_c t - i\phi_c(t)}\sigma_{mm} + e^{-i\omega_p t - i\phi_p(t)}\sigma_{gg}$ and using $\dot{\phi}_{c(p)}(t) = \mu_{c(p)}(t)$, the Hamiltonian becomes $H_U = i\dot{U}U^\dagger + UHU^\dagger = H_1 + H_2$, with

$$H_1 = -\delta_c\sigma_{mm} - \delta_p\sigma_{gg} - \Omega_c\sigma_{em} - \Omega_p\sigma_{eg} + \text{H.c.}, \tag{5a}$$

$$H_2 = \delta\omega_e(t)\sigma_{ee} + [\delta\omega_m(t) + \mu_c(t)]\sigma_{mm} + \mu_p(t)\sigma_{gg}. \tag{5b}$$

Here, $U(t)$ can be regarded as a transformation to a rotating frame with random phases. (If we ignore $\phi_{c(p)}(t)$, $U(t)$ represents a transformation to a usual rotating frame.) The master equation is

$$\dot{\rho} = -i[H_1, \rho] - i[H_2, \rho] - \mathcal{L}_{\text{vac}}\rho, \tag{6}$$

with

$$\mathcal{L}_{\text{vac}}\rho = \frac{\Gamma}{2}(\sigma_{ee}\rho + \rho\sigma_{ee}) - \Gamma_{em}\rho_{ee}\sigma_{mm} - \Gamma_{eg}\rho_{ee}\sigma_{gg}. \tag{7}$$

According to the theory of multiplicative stochastic processes [47], the equation of motion of the average ρ is obtained:

$$\langle\dot{\rho}\rangle = -i[H_1, \langle\rho\rangle] - \mathcal{L}_{\text{vac}}\langle\rho\rangle - \int_0^t d\tau \langle[H_2(t), [H_2(\tau), \rho]]\rangle$$

$$= -i[H_1, \langle\rho\rangle] - \mathcal{L}_{\text{vac}}\langle\rho\rangle - \mathcal{L}_{\text{col}}\langle\rho\rangle - \mathcal{L}_{\text{ph}}\langle\rho\rangle, \tag{8}$$

with

$$\mathcal{L}_{\text{col}}\langle\rho\rangle = \gamma_e^{(d)}[\sigma_{ee}, [\sigma_{ee}, \langle\rho\rangle]] + \gamma_m^{(d)}[\sigma_{mm}, [\sigma_{mm}, \langle\rho\rangle]], \tag{9}$$

$$\mathcal{L}_{\text{ph}}\langle\rho\rangle = \kappa_c^{(d)}[\sigma_{mm}, [\sigma_{mm}, \langle\rho\rangle]] + \kappa_p^{(d)}[\sigma_{gg}, [\sigma_{gg}, \langle\rho\rangle]]$$
$$+ \zeta_{cp}\sqrt{\kappa_c^{(d)}\kappa_p^{(d)}} \left([\sigma_{mm}, [\sigma_{gg}, \langle\rho\rangle]] + [\sigma_{gg}, [\sigma_{mm}, \langle\rho\rangle]]\right). \tag{10}$$

The first term in Eq. (8) describes the coherent interaction inducing the atomic coherences, which are represented by the off-diagonal elements ρ_{ij}. $\mathcal{L}_{\text{vac}}\langle\rho\rangle$ represents the spontaneous decay due to the vacuum fluctuation. $\mathcal{L}_{\text{col}}\langle\rho\rangle$ and $\mathcal{L}_{\text{ph}}\langle\rho\rangle$ give the dephasing induced by the atomic collisions and the field phase diffusions, respectively. The decoherence rate of ρ_{ij} is $\gamma_{ij} = \langle i|(\mathcal{L}_{\text{vac}}\langle\rho\rangle + \mathcal{L}_{\text{col}}\langle\rho\rangle + \mathcal{L}_{\text{ph}}\langle\rho\rangle)|j\rangle/\langle\rho_{ij}\rangle$, and we have

$$\gamma_{em} = \frac{\Gamma}{2} + \gamma_{em}^{(D)}, \quad \gamma_{eg} = \frac{\Gamma}{2} + \gamma_{eg}^{(D)}, \quad \gamma_{mg} = \gamma_{mg}^{(D)}, \tag{11}$$

with the dephasing rates

$$\gamma_{em}^{(D)} = \gamma_e^{(d)} + \gamma_m^{(d)} + \kappa_c^{(d)}, \tag{12a}$$

$$\gamma_{eg}^{(D)} = \gamma_e^{(d)} + \kappa_p^{(d)}, \tag{12b}$$

$$\gamma_{mg}^{(D)} = \gamma_m^{(d)} + \kappa_c^{(d)} + \kappa_p^{(d)} - 2\zeta_{cp}\sqrt{\kappa_c^{(d)}\kappa_p^{(d)}}. \tag{12c}$$

Equations (11) and (12) show that the decoherence of the atom–field system originates from (i) spontaneous decay ($\Gamma/2$); (ii) atomic-collision-induced dephasing ($\gamma_{e(m)}^{(d)}$); (iii) field-phase-diffusion-induced dephasing ($\kappa_{c(p)}^{(d)}$); and (iv) field-phase-correlation-induced dephasing ($-2\zeta_{cp}\sqrt{\kappa_c^{(d)}\kappa_p^{(d)}}$), which takes negative value for $\zeta_{cp} > 0$ or positive value for $\zeta_{cp} < 0$, implying that the phase correlation can weaken or enhance the dephasing between the lower states $|m\rangle$ and $|g\rangle$.

The QI and ATS effects coexist in the present atom–field system and are influenced by the dephasing. In the following discussion, we focus our attention on the influence of dephasing on the relative weights of QI and ATS. The discussion also shows the possibility to control the weights via manipulating the dephasing with the phase correlation of fields.

3. INFLUENCE OF DEPHASING ON THE RELATIVE WEIGHTS OF QI AND ATS

The absorption spectrum of the probe field is determined by the imaginary part of the susceptibility χ, which is proportional to atomic coherence ρ_{eg}. Here, we consider the case of $\delta_c = 0$ for the resonant coupling field. By solving the steady-state solution ($\langle\dot{\rho}\rangle = 0$) of Eq. (8), we obtain the susceptibility

$$\chi = \frac{N_a d_{eg}}{\varepsilon_0 \mathcal{E}_p}\langle\rho_{eg}\rangle = \kappa \frac{\delta_p - i\gamma_{mg}}{(\delta_p - i\gamma_{eg})(\delta_p - i\gamma_{mg}) - \Omega_c^2}, \tag{13}$$

with $\kappa = N_a d_{eg}^2/\varepsilon_0$, atomic number density N_a, and vacuum permittivity ε_0. χ has two poles $\delta_\pm = ig \pm i\sqrt{\eta^2 - \Omega_c^2}$ and thus can be decomposed as

$$\chi = \kappa\frac{\delta_p - i\gamma_{mg}}{(\delta_p - \delta_+)(\delta_p - \delta_-)} = \frac{\kappa}{2}\left(\frac{J_+}{\delta_p - \delta_+} + \frac{J_-}{\delta_p - \delta_-}\right), \tag{14}$$

where $J_\pm = 1 \pm \eta/\sqrt{\eta^2 - \Omega_c^2}$, with $\eta = (\gamma_{eg} - \gamma_{mg})/2$ and $g = (\gamma_{eg} + \gamma_{mg})/2$. The term $\sqrt{\eta^2 - \Omega_c^2}$ is a real or imaginary number for $|\eta| > \Omega_c$ or $|\eta| < \Omega_c$, giving rise to different forms of χ. Here, we consider the absorption spectrum under the conditions of $|\eta| > \Omega_c$, $|\eta| \sim \Omega_c$, and $|\eta| \ll \Omega_c$.

(i) For $|\eta| > \Omega_c$, the absorption spectrum can be written as

$$\alpha_{\text{QI}} = \alpha_{\text{Q1}} + \alpha_{\text{Q2}}$$

$$= \frac{\kappa}{2}\left[\frac{\left(1 + \eta/\sqrt{\eta^2 - \Omega_c^2}\right)\left(g + \sqrt{\eta^2 - \Omega_c^2}\right)}{\delta_p^2 + \left(g + \sqrt{\eta^2 - \Omega_c^2}\right)^2}\right.$$

$$\left. + \frac{\left(1 - \eta/\sqrt{\eta^2 - \Omega_c^2}\right)\left(g - \sqrt{\eta^2 - \Omega_c^2}\right)}{\delta_p^2 + \left(g - \sqrt{\eta^2 - \Omega_c^2}\right)^2}\right]. \tag{15}$$

The absorption spectrum α_{QI}, as shown by the black line in Fig. 2(a), is a result of the overlapping of wider positive α_{Q1}
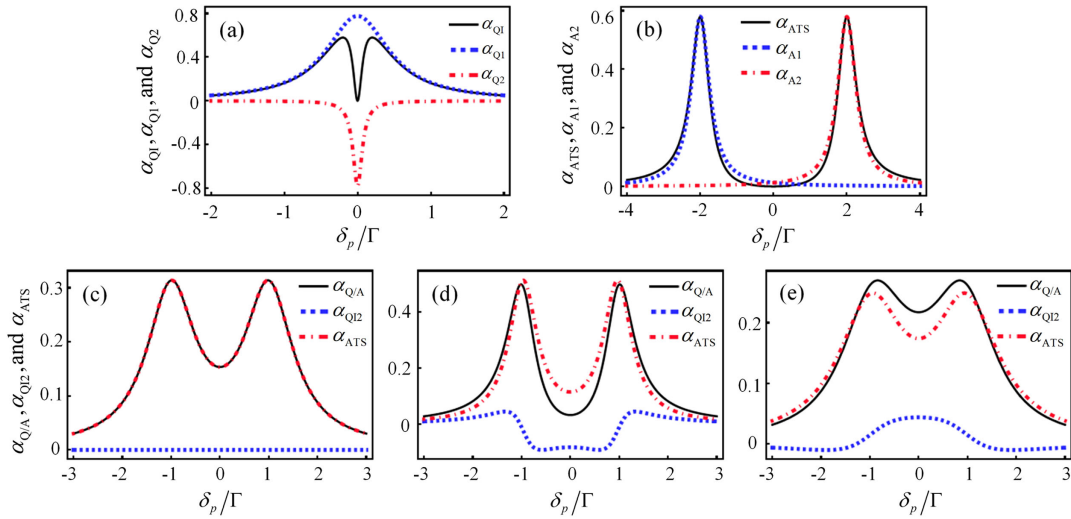
Fig. 2. (a), (b) Absorption spectra for $\Omega_c = 0.2\Gamma$ (a) and $\Omega_c = 2\Gamma$ (b) with $\gamma_{mg}^{(D)} = 0$. (c)–(e) Absorption spectra with $\Omega_c = \Gamma$ when $\gamma_{mg}^{(D)} = 0.6\Gamma$ (c), $\gamma_{mg}^{(D)} = 0.1\Gamma$ (d), and $\gamma_{mg}^{(D)} = \Gamma$ (e), corresponding to $\eta = 0$, 0.25Γ, and -0.2Γ, respectively. The other parameter is $\gamma_{eg}^{(D)} = 0.1\Gamma$.

(blue line) and narrower negative α_{Q2} (red line) Lorentzian profiles, leading to the absorption suppression at resonance, i.e., EIT. In this case, the EIT absorption spectrum is considered as the QI effect.

(ii) For $|\eta| \ll \Omega_c$, the absorption spectrum [black line in Fig. 2(b)] is simply a superposition of two independent Lorentzian profiles of α_{A1} and α_{A2} (blue and red lines):

$$\alpha_{ATS} = \alpha_{A1} + \alpha_{A2}$$

$$= \frac{\kappa}{2} \left[\frac{g}{\left(\delta_p + \sqrt{\Omega_c^2 - \eta^2}\right)^2 + g^2} + \frac{g}{\left(\delta_p - \sqrt{\Omega_c^2 - \eta^2}\right)^2 + g^2} \right]. \tag{16}$$

These two Lorentzian profiles are located at $\pm\sqrt{\Omega_c^2 - \eta^2} \approx \pm\Omega_c$ with the same linewidth g. In this case, the system exhibits an ATS feature without interference [50].

(iii) For $|\eta| \sim \Omega_c$, the absorption spectrum can be expressed as

$$\alpha_{Q/A} = \alpha_{ATS} + \alpha_{QI2} = \frac{\kappa}{2} \left[\frac{g}{\left(\delta_p + \sqrt{\Omega_c^2 - \eta^2}\right)^2 + g^2} + \frac{g}{\left(\delta_p - \sqrt{\Omega_c^2 - \eta^2}\right)^2 + g^2} \right]$$

$$+ \frac{\kappa}{2} \frac{\eta}{\sqrt{\Omega_c^2 - \eta^2}} \left[\frac{\delta_p + \sqrt{\Omega_c^2 - \eta^2}}{\left(\delta_p + \sqrt{\Omega_c^2 - \eta^2}\right)^2 + g^2} + \frac{\delta_p - \sqrt{\Omega_c^2 - \eta^2}}{\left(\delta_p - \sqrt{\Omega_c^2 - \eta^2}\right)^2 + g^2} \right]. \tag{17}$$

The first two Lorentzian profiles are exactly the same expression α_{ATS} of ATS in Eq. (16), and the last two terms (denoted by α_{QI2}) are therefore related to the terms for QI. When $\eta = \Gamma/4 + (\gamma_{eg}^{(D)} - \gamma_{mg}^{(D)})/2 = 0$, α_{QI2} vanishes, and the absorption is completely determined by ATS [see Fig. 2(c)]. When $\eta \neq 0$, both QI and ATS terms (α_{QI2} and α_{ATS}) have influences on the absorption, and one cannot readout which one is dominant. Note that the QIs for $\eta > 0$ and $\eta < 0$ are different. When $\eta > 0$, as shown in Fig. 2(d), compared to the ATS absorption (α_{ATS}, red line), the total absorption ($\alpha_{Q/A}$,

black line) is suppressed, representing destructive QI (DQI), i.e., EIT. On the other hand, when $\eta < 0$, as shown in Fig. 2(e), the total absorption ($\alpha_{Q/A}$, black line) is stronger than the ATS absorption (α_{ATS}, red line), i.e., constructive QI (CQI).

In order to differentiate QI and ATS, the AIC is adopted to evaluate their relative weights quantitatively. For i) QI and ii) ATS cases, the absorption spectra can be rewritten as

$$\alpha_{QI} = \frac{C_1^2}{\delta_p^2 + \xi_1^2} - \frac{C_2^2}{\delta_p^2 + \xi_2^2}, \tag{18a}$$

$$\alpha_{ATS} = \frac{C^2}{(\delta_p - \delta_1)^2 + \xi^2} + \frac{C^2}{(\delta_p + \delta_1)^2 + \xi^2}, \tag{18b}$$

where the parameters $C_{1(2)}$, C, $\xi_{1(2)}$, ξ, and δ_1 can be calculated from Eqs. (15) and (16). One can use these two approximation models α_{QI} and α_{ATS} to fit the experimental data with fitting parameters $C_{1(2)}$, C, $\xi_{1(2)}$, ξ, and δ_1. The AIC of $\alpha_{QI(ATS)}$ is defined as $I_{QI(ATS)} = 2K_{QI(ATS)} - 2\log L_{QI(ATS)}$ [37,38],

where $K_{QI(ATS)} = 4(3)$ is the number of fitting parameters, and $L_{QI(ATS)}$ is the maximum of the likelihood function. The relative weight of $\alpha_{QI(ATS)}$ is given by the per-point Akaike weight

$$w_{QI(ATS)} = \frac{e^{-I_{QI(ATS)}/2N}}{e^{-I_{QI}/2N} + e^{-I_{ATS}/2N}}, \tag{19}$$

with the number of fitting points N, and $w_{QI} + w_{ATS} = 1$. Akaike weight $w_{QI(ATS)}$ quantitatively represents how well

$\alpha_{\mathrm{QI(ATS)}}$ fits the experimental data and thus determines the relative weight of the QI (ATS) effect. $w_{\mathrm{QI(ATS)}}$ increasing from 0 to 1 means that QI (ATS) becomes stronger.

Here, we use the model Im χ [see Eq. (13)] to simulate the experimental data to be fitted by $\alpha_{\mathrm{QI(ATS)}}$. The calculated Akaike weight $w_{\mathrm{QI(ATS)}}$ now represents how close $\alpha_{\mathrm{QI(ATS)}}$ is to Im χ. As an example, in Fig. 3, we use α_{QI} and α_{ATS} (blue and red lines) to fit the simulated data (black lines), and calculate their Akaike weights w_{QI} and w_{ATS}, respectively. It can be seen that decreasing $|\eta|$ or increasing Ω_c makes QI weaker and ATS stronger.

Figures 4 and 5 display the dependences of the QI and ATS weights (w_{QI} and w_{ATS}) on the atomic-collision-induced dephasing ($\gamma_e^{(\mathrm{d})}$ and $\gamma_m^{(\mathrm{d})}$) and field-phase-diffusion-induced dephasing ($\kappa_c^{(\mathrm{d})}$, $\kappa_p^{(\mathrm{d})}$, and ζ_{cp}), respectively. We consider the three conditions: (i) $\eta = 0$ for a boundary of DQI and CQI, as denoted by the solid white lines in Figs. 4 and 5, for which $|\eta| \ll \Omega_c$, and thus the absorption spectrum is determined by ATS without QI, i.e., $w_{\mathrm{ATS}} = 1$ and $w_{\mathrm{QI}} = 0$. (ii) $\eta > 0$ for absorption suppression with DQI. (iii) $\eta < 0$ for enhanced absorption with CQI. As $|\eta|$ increases, w_{QI} increases while w_{ATS} decreases. In other words, one obtains strong QI in the region far away from the boundary. In the region of $\eta > 0$ ($\eta < 0$), QI is destructive (constructive), resulting in a suppressed (enhanced) resonant absorption, as analyzed above. Therefore, $|\eta|$ determines the strength of QI, and the sign of η gives the nature of QI. Also note that w_{QI} becomes smaller for a larger Ω_c regardless of the values of dephasing rates (see the change from the second column to the last column in Figs. 4 and 5), which is in consistent with the previous studies [24,25].

The white dashed lines in Figs. 4 and 5 denote $w_{\mathrm{QI}} = w_{\mathrm{ATS}} = 0.5$, which is the critical condition for the transition from QI to ATS. In the range from $w_{\mathrm{QI}} = 0$ (solid white lines) to $w_{\mathrm{QI}} = 0.5$ (dashed white lines), the ATS effect dominates, while in the range $w_{\mathrm{QI}} > 0.5$, the QI effect dominates. This critical condition depends on the dephasing rates ($\gamma_{e(m)}^{(\mathrm{d})}$, $\kappa_{c(p)}^{(\mathrm{d})}$, and ζ_{cp}) and the coupling Rabi frequency (Ω_c), and thus can be considered as a criterion to differentiate QI and ATS from experimental parameters.

By comparing Figs. 4 and 5, it is seen that the field-phase-diffusion-induced dephasing is more flexible than atomic-collision-induced dephasing in control of the weights of QI and ATS. Experimentally, the collisional dephasing rates are generally adjusted by changing the partial pressure of the buffer gas filled in the atomic vapor. It is difficult to get the exact values of dephasing rates, and one cannot adjust only $\gamma_e^{(\mathrm{d})}$ ($\gamma_m^{(\mathrm{d})}$) while keeping $\gamma_m^{(\mathrm{d})}$ ($\gamma_e^{(\mathrm{d})}$) unchanged. Instead, it is much easier to adjust the laser linewidths and correlation coefficients using the phase modulation and locking techniques. Thus, the field-phase-diffusion-induced dephasing can be precisely and selectively controlled. Also, the field-phase-diffusion-induced dephasing has more degrees of freedom than atomic-collision-induced dephasing. Apart from the phase diffusion rates ($\kappa_c^{(\mathrm{d})}$ and $\kappa_p^{(\mathrm{d})}$), the phase correlation between the coupling and probe fields is crucial for manipulation of w_{QI} and w_{ATS}. As the correlation coefficient ζ_{cp} changes from 1 (complete correlation) to -1 (complete anti-correlation), the region of DQI ($\eta > 0$) becomes small, while the region of CQI ($\eta < 0$) becomes large (see the change from the first row to the last row in Fig. 5),
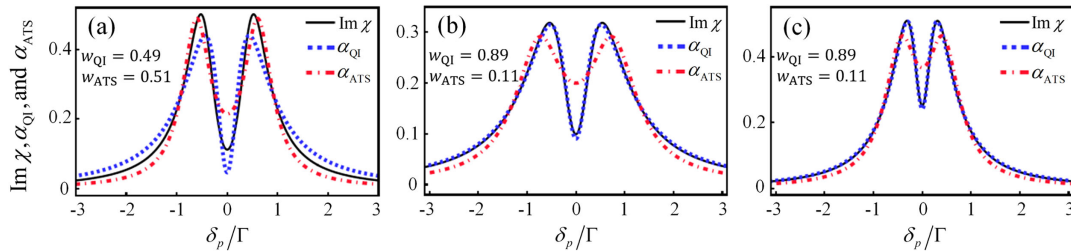

Fig. 3. Fitting the absorption spectra to get the relative weights of QI and ATS when (a) $\Omega_c = 0.5\Gamma$, $\gamma_{eg}^{(\mathrm{D})} = 0.1\Gamma$ ($\eta = 0.25\Gamma$); (b) $\Omega_c = 0.5\Gamma$, $\gamma_{eg}^{(\mathrm{D})} = 0.5\Gamma$ ($\eta = 0.45\Gamma$); and (c) $\Omega_c = 0.28\Gamma$, $\gamma_{eg}^{(\mathrm{D})} = 0.1\Gamma$ ($\eta = 0.25\Gamma$). The other parameter is $\gamma_{mg}^{(\mathrm{D})} = 0.1\Gamma$.
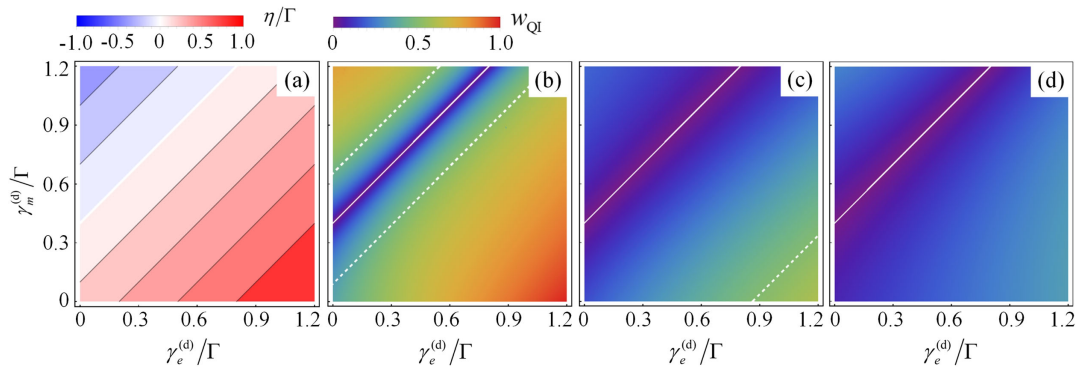

Fig. 4. Dependences of (a) η and (b)–(d) w_{QI} ($w_{\mathrm{ATS}} = 1 - w_{\mathrm{QI}}$) on $\gamma_m^{(\mathrm{d})}$ and $\gamma_e^{(\mathrm{d})}$ with (b) $\Omega_c = 0.8\Gamma$, (c) $\Omega_c = 1.5\Gamma$, and (d) $\Omega_c = 3\Gamma$. The white lines indicate $\eta = 0$ ($w_{\mathrm{QI}} = 0$ and $w_{\mathrm{ATS}} = 1$), and the solid white dashed lines indicate $w_{\mathrm{QI}} = w_{\mathrm{ATS}} = 0.5$. The other parameters are $\kappa_c^{(\mathrm{d})} = \kappa_p^{(\mathrm{d})} = 0.1\Gamma$ and $\zeta_{cp} = 0$.
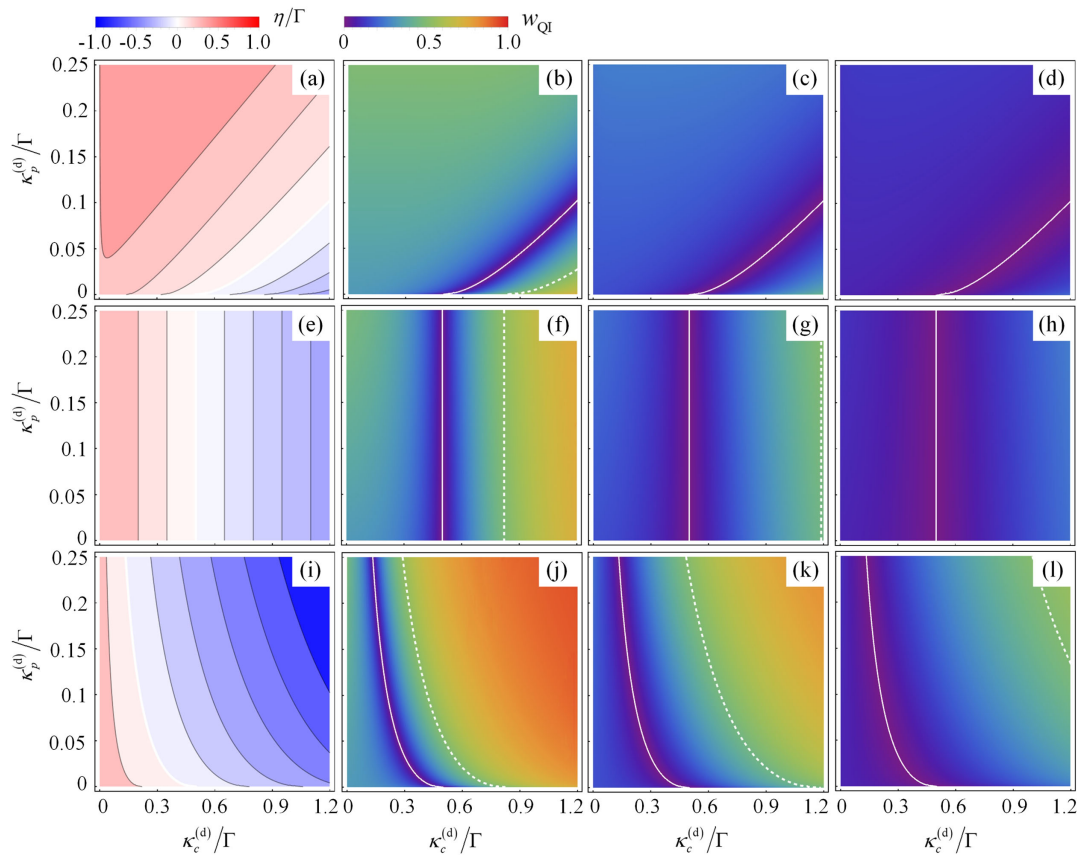
Fig. 5. Dependences of η (first column) and w_{QI} ($w_{\mathrm{ATS}} = 1 - w_{\mathrm{QI}}$) (second to fourth columns) on $\kappa_c^{(\mathrm{d})}$ and $\kappa_p^{(\mathrm{d})}$ with (b), (f), and (j) $\Omega_c = 0.8\Gamma$; (c), (g), and (k) $\Omega_c = 1.5\Gamma$; (d), (h), and (l) $\Omega_c = 3\Gamma$. The phase-correlation coefficient $\zeta_{cp} = 1$ (first row), 0 (second row), and -1 (third row). The solid white lines indicate $\eta = 0$ ($w_{\mathrm{QI}} = 0$ and $w_{\mathrm{ATS}} = 1$), and the white dashed lines indicate $w_{\mathrm{QI}} = w_{\mathrm{ATS}} = 0.5$. The other parameters are $\gamma_e^{(\mathrm{d})} = \gamma_m^{(\mathrm{d})} = 0.02\Gamma$.

i.e., one can use phase-correlated coupling and probe fields to improve QI.

4. CONCLUSION

Using the theory of multiplicative stochastic processes, we have investigated the dephasing effect of an atom–field system involving atom–atom collisions and field phase diffusion, and have obtained the corresponding dephasing rates. Based on this and utilizing AIC, we have studied the influences of atom-collision dephasing and field-phase-diffusion dephasing on the relative weights of QI and ATS. The transition among DQI (EIT), CQI (EIA), and ATS without QI can be obtained via changing the dephasing rates. The continuously and selectively controllable features of the field-phase-diffusion dephasing provide a way to realize the precise dephasing engineering via manipulating the linewidths and phase correlation of fields. Previous discussions focus mainly on the influence of coupling Rabi frequency on QI and ATS weights. In this discussion, we have highlighted the role of dephasing rates for distinguishing QI and ATS.

Disclosures. The authors declare no conflicts of interest.

REFERENCES

1. M. Fleischhauer, A. Imamoğlu, and J. P. Marangos, "Electromagnetically induced transparency: optics in coherent media," Rev. Mod. Phys. **77**, 633–673 (2005).
2. S. E. Harris, J. E. Field, and A. Imamoğlu, "Nonlinear optical processes using electromagnetically induced transparency," Phys. Rev. Lett. **64**, 1107–1110 (1990).
3. K. J. Boller, A. Imamoğlu, and S. E. Harris, "Observation of electromagnetically induced transparency," Phys. Rev. Lett. **66**, 2593–2596 (1991).
4. C. Monroe, "Quantum information processing with atoms and photons," Nature **416**, 238–246 (2002).
5. M. Saffman, T. G. Walker, and K. Mølmer, "Quantum information with Rydberg atoms," Rev. Mod. Phys. **82**, 2313–2363 (2010).
6. J. Appel, P. J. Windpassinger, D. Oblak, U. B. Hoff, N. Kjærgaard, and E. S. Polzik, "Mesoscopic atomic entanglement for precision measurements beyond the standard quantum limit," Proc. Natl. Acad. Sci. **106**, 10960–10965 (2009).
7. J. Ye, H. J. Kimble, and H. Katori, "Quantum state engineering and precision metrology using state-insensitive light traps," Science **320**, 1734–1738 (2008).
8. N. Hinkley, J. A. Sherman, N. B. Phillips, M. Schioppo, N. D. Lemke, K. Beloy, M. Pizzocaro, C. W. Oates, and A. D. Ludlow, "An atomic clock with 10⁻¹⁸ instability," Science **341**, 1215–1218 (2013).

9. L. V. Hau, E. S. Harris, Z. Dutton, and C. H. Behroozi, "Light speed reduction to 17 metres per second in an ultracold atomic gas," Nature **397**, 594–598 (1999).

10. D. Budker, D. F. Kimball, S. M. Rochester, and V. V. Yashchuk, "Nonlinear magneto-optics and reduced group velocity of light in atomic vapor with slow ground state relaxation," Phys. Rev. Lett. **83**, 1767–1770 (1999).

11. D. F. Phillips, A. Fleischhauer, A. Mair, R. L. Walsworth, and M. D. Lukin, "Storage of light in atomic vapor," Phys. Rev. Lett. **86**, 783–786 (2001).

12. Y. F. Hsiao, P. J. Tsai, H. S. Chen, S. X. Lin, C. C. Hung, C. H. Lee, Y. H. Chen, Y. F. Chen, I. A. Yu, and Y. C. Chen, "Highly efficient coherent optical memory based on electromagnetically induced transparency," Phys. Rev. Lett. **120**, 183602 (2018).

13. B. Julsgaard, J. Sherson, J. I. Cirac, J. Fiurášek, and E. S. Polzik, "Experimental demonstration of quantum memory for light," Nature **432**, 482–486 (2004).

14. Y. O. Dudin, L. Li, and A. Kuzmich, "Light storage on the time scale of a minute," Phys. Rev. A **87**, 031801(R) (2013).

15. G. Heinze, C. Hubrich, and T. Halfmann, "Stopped light and image storage by electromagnetically induced transparency up to the regime of one minute," Phys. Rev. Lett. **111**, 033601 (2013).

16. A. M. Marino, R. C. Pooser, V. Boyer, and P. D. Lett, "Tunable delay of Einstein-Podolsky-Rosen entanglement," Nature **457**, 859–862 (2009).

17. C. F. McCormick, V. Boyer, E. Arimondo, and P. D. Lett, "Strong relative intensity squeezing by four-wave mixing in rubidium vapor," Opt. Lett. **32**, 178–180 (2007).

18. V. Boyer, A. M. Marino, R. C. Pooser, and P. D. Lett, "Entangled images from four-wave mixing," Science **321**, 544–547 (2008).

19. M.-J. Guo, H.-T. Zhou, D. Wang, J.-R. Gao, J.-X. Zhang, and S.-Y. Zhu, "Experimental investigation of high-frequency-difference twin beams in hot cesium atoms," Phys. Rev. A **89**, 033813 (2014).

20. A. Christofi, Y. Kawaguchi, A. Alù, and A. B. Khanikaev, "Giant enhancement of Faraday rotation due to electromagnetically induced transparency in all-dielectric magneto-optical metasurfaces," Opt. Lett. **43**, 1838–1841 (2018).

21. C. Y. Hu, S. A. Schulz, A. A. Liles, and L. O'Faolain, "Tunable optical buffer through an analogue to electromagnetically induced transparency in coupled photonic crystal cavities," ACS Photon. **5**, 1827–1832 (2018).

22. L.-J. Yang, L.-S. Zhang, X.-L. Li, L. Han, G.-S. Fu, N. B. Manson, D. Suter, and C.-J. Wei, "Autler-Townes effect in a strongly driven electromagnetically induced transparency resonance," Phys. Rev. A **72**, 053801 (2005).

23. T. Y. Abi-Salloum, "Electromagnetically induced transparency and Autler-Townes splitting: Two similar but distinct phenomena in two categories of three-level atomic systems," Phys. Rev. A **81**, 053836 (2010).

24. P. M. Anisimov, J. P. Dowling, and B. C. Sanders, "Objectively discerning Autler-Townes splitting from electromagnetically induced transparency," Phys. Rev. Lett. **107**, 163604 (2011).

25. L. Giner, L. Veissier, B. Sparkes, A. S. Sheremet, A. Nicolas, O. S. Mishina, M. Scherman, S. Burks, I. Shomroni, D. V. Kupriyanov, and P. K. Lam, "Experimental investigation of the transition between Autler-Townes splitting and electromagnetically-induced-transparency models," Phys. Rev. A **87**, 013823 (2013).

26. S. H. Autler and C. H. Townes, "Stark effect in rapidly varying fields," Phys. Rev. **100**, 703–722 (1955).

27. C. N. Cohen-Tannoudji, "The Autler-Townes effect revisited," in Amazing Light (Springer, 1996), pp. 109–123.

28. D. J. Wineland and W. M. Itano, "Laser cooling of atoms," Phys. Rev. A **20**, 1521–1540 (1979).

29. C. G. Wade, N. Šibalić, J. Keaveney, C. S. Adams, and K. J. Weatherill, "Probing an excited-state atomic transition using hyperfine quantum-beat spectroscopy," Phys. Rev. A **90**, 033424 (2014).

30. C. L. Holloway, J. A. Gordon, A. Schwarzkopf, D. A. Anderson, S. A. Miller, N. Thaicharoen, and G. Raithel, "Sub-wavelength imaging and field mapping via electromagnetically induced transparency and Autler-Townes splitting in Rydberg atoms," Appl. Phys. Lett. **104**, 244102 (2014).

31. E. Saglamyurek, T. Hrushevskyi, A. Rastogi, K. Heshami, and L. J. LeBlanc, "Coherent storage and manipulation of broadband photons via dynamically controlled Autler-Townes splitting," Nat. Photonics **12**, 774–782 (2018).

32. P. Anisimov and O. Kocharovskaya, "Decaying-dressed-state analysis of a coherently driven three-level Λ system," J. Mod. Opt. **55**, 3159–3171 (2008).

33. C.-J. Zhu, C.-H. Tan, and G.-X. Huang, "Crossover from electromagnetically induced transparency to Autler-Townes splitting in open V-type molecular systems," Phys. Rev. A **87**, 043813 (2013).

34. B. Peng, Ş. K. Özdemir, W.-J. Chen, F. Nori, and L. Yang, "What is and what is not electromagnetically induced transparency in whispering-gallery microcavities," Nat. Commun. **5**, 5082 (2014).

35. L.-Y. He, T.-J. Wang, Y.-P. Gao, C. Cao, and C. Wang, "Discerning electromagnetically induced transparency from Autler-Townes splitting in plasmonic waveguide and coupled resonators system," Opt. Express **23**, 23817–23826 (2015).

36. Q.-C. Liu, T.-F. Li, X.-Q. Luo, H. Zhao, W. Xiong, Y.-S. Zhang, Z. Chen, J. S. Liu, W. Chen, F. Nori, J. S. Tsai, and J. Q. You, "Method for identifying electromagnetically induced transparency in a tunable circuit quantum electrodynamics system," Phys. Rev. A **93**, 053838 (2016).

37. K. P. Burnham and D. R. Anderson, Model Selection and Multimodel Inference: A Practical Information-Theoretic Approach (Springer, 2003).

38. H. Akaike, "A new look at the statistical model identification," IEEE Trans. Autom. Control **19**, 716–723 (1974).

39. X. Yang, J. Sheng, and M. Xiao, "Electromagnetically induced absorption via incoherent collisions," Phys. Rev. A **84**, 043837 (2011).

40. M. T. Graf, D. F. Kimball, S. M. Rochester, K. Kerner, C. Wong, D. Budker, E. B. Alexandrov, M. V. Balabas, and V. V. Yashchuk, "Relaxation of atomic polarization in paraffin-coated cesium vapor cells," Phys. Rev. A **72**, 023401 (2005).

41. J. Borregaard, M. Zugenmaier, J. M. Petersen, H. Shen, G. Vasilakis, K. Jensen, E. S. Polzik, and A. S. Sørensen, "Scalable photonic network architecture based on motional averaging in room temperature gas," Nat. Commun. **7**, 11356 (2016).

42. P. Peng, W. Cao, C. Shen, W. Qu, J. Wen, L. Jiang, and Y. Xiao, "Anti-parity-time symmetry with flying atoms," Nat. Phys. **12**, 1139–1145 (2016).

43. D. A. Steck, "Cesium D line data," 2010, http://steck.us/alkalidata.

44. P. J. Leo, P. S. Julienne, F. H. Mies, and C. J. Williams, "Collisional frequency shifts in ^{133}Cs fountain clocks," Phys. Rev. Lett. **86**, 3743–3746 (2001).

45. D. M. Harber, H. J. Lewandowski, J. M. McGuirk, and E. A. Cornell, "Effect of cold collisions on spin coherence and resonance shifts in a magnetically trapped ultracold gas," Phys. Rev. A **66**, 053616 (2002).

46. K. Gibble and S. Chu, "Laser-cooled Cs frequency standard and a measurement of the frequency shift due to ultracold collisions," Phys. Rev. Lett. **70**, 1771–1774 (1993).

47. G. S. Agarwal, "Quantum statistical theory of optical-resonance phenomena in fluctuating laser fields," Phys. Rev. A **18**, 1490–1506 (1978).

48. J. Benesty, J.-D. Chen, and Y.-T. Huang, "On the importance of the Pearson correlation coefficient in noise reduction," IEEE Trans. Audio Speech Lang. Process. **16**, 757–765 (2008).

49. J. Benesty, J.-D. Chen, Y.-T. Huang, and I. Cohen, "Pearson correlation coefficient," in Noise Reduction in Speech Processing (Springer, 2009), pp. 37–40.

50. G. S. Agarwal, "Nature of the quantum interference in electromagnetic-field-induced control of absorption," Phys. Rev. A **55**, 2467–2470 (1997).